Sum frequency generation, calculation of absolute intensities, comparison with experiments, and two-field relaxation-based derivation

Kai Niu[a,b] and Rudolph A. Marcus[b,1]

[a]School of Science, Tianjin University of Technology and Education, Hexi, Tianjin 300222, People's Republic of China; and [b]Noyes Laboratory of Chemical Physics, California Institute of Technology, Pasadena, CA 91125

Contributed by Rudolph A. Marcus, December 15, 2019 (sent for review April 12, 2019; reviewed by Shaul Mukamel and Francesco Paesani)

The experimental sum frequency generation (SFG) spectrum is the response to an infrared pulse and a visible pulse and is a highly surface-sensitive technique. We treat the surface dangling OH bonds at the air/water interface and focus on the absolute SFG intensities for the resonant terms, a focus that permits insight into the consequences of some approximations. For the polarization combinations, the calculated linewidths for the water interface dangling OH SFG band at 3,700 cm^{-1} are, as usual, too large, because of the customary neglect of motional narrowing. The integrated spectrum is used to circumvent this problem and justified here using a Kubo-like formalism and theoretical integrated band intensities rather than peak intensities. Only relative SFG intensities are usually reported. The absolute integrated SFG intensities for three polarization combinations for sum frequency, visible, and infrared beams are computed. We use molecular dynamics and the dipole and the polarizability matrix elements obtained from infrared and Raman studies of H_2O vapor. The theoretical expressions for two of the absolute susceptibilities contain only a single term and agree with experiment to about a factor of 1.3, with no adjustable parameters. The Fresnel factors are included in that comparison. One of the susceptibilities contains instead four positive and negative terms and agrees less well. The expression for the SFG correlation function is normally derived from a statistical mechanical formulation using a time-evolving density matrix. We show how a derivation based on a two-field relaxation leads to the same final result.

sum frequency generation | integrated spectrum | SFG | motional narrowing | absolute intensities

Sum frequency generation (SFG), one of the second-order nonlinear spectroscopies, was developed to study the properties of interfaces, such as those involving air/water interfaces (1–61). In SFG experiments, there are two incident laser pulses with identical or different polarizations, the frequency of one laser beam being in the infrared (IR) and the other in the visible. The two beams are mixed in the present case at an air/water interface, while the output signal is collected in the sum frequency direction. The polarization combinations for sum frequency, visible, and infrared beams studied by Wei and Shen (3) are written as ssp, sps, and ppp, where, for example, ssp denotes that the sum frequency output and the visible input beams are both s polarized; i.e., their electric field vectors are parallel to the surface. The p denotes that the infrared input beam is p polarized; that is, the electric field lies in the plane perpendicular to the interface.

SFG has proved to be a particularly useful experimental tool for the study of interfaces, e.g., air/water surfaces (1–33), and has been studied theoretically and computationally (34–61). In the computations typically classical trajectories are used (34–46, 55, 56), often with some quantum correction for the vibrations.

One goal of the present paper is to calculate absolute SFG intensities for the different polarization combinations, using data from infrared and Raman experiments, and compare them with the absolute intensities for the SFG experimental results, correcting for their Fresnel factors in the comparison. A motivation of the present study was the study of the dangling interfacial OH bonds that play a role in the catalysis of "on-water" reactions in emulsions (62, 63). Typically the derivation of an expression of the frequency-dependent SFG and for other susceptibilities is made using perturbation theory (41, 57, 58, 64). In a single-laser system the frequency-dependent susceptibility has also been obtained by studying the relaxation of the system after introducing a step function in the external force (e.g., electric field) and then allowing the system to relax after removal of the field (65). In the present case there are two electric fields involved in the relaxation, one of which interacts with the electrons (it corresponds to the Raman source) and the other one interacts with the nuclei (it corresponds to the infrared source). The relaxation method is modified here to treat this two–electric-field system.

Usually in deriving the value of a time-correlation function for SFG the matrix elements are computed separately or, when obtaining an absolute value for the SFG susceptibility is not a goal, the absolute values of those matrix elements are either not considered or estimated approximately, perhaps with classical molecular dynamics (MD) with a quantum correction (42, 56, 57). For providing detailed information on the SFG, the MD technique was developed (34–46) as well as recently an efficient calculation algorithm for computing the SFG spectra

Significance

The water surface structures, where a dangling OH bond plays a role in catalysis, can be studied by the sum frequency generation (SFG) experimentally and theoretically. The dangling OH bond region of the SFG is investigated using the classical molecular dynamics simulation for the ssp, sps, and ppp combinations of the different electric field polarizations. Reasonable agreement with no adjustable parameters within a factor of 1.3 is obtained with the experimental single-term SFG polarization combinations ssp and sps. The comparison of the calculated absolute SFG intensities with the experimental values provides a test of the various approximations in the literature, such as the values used in some cases for the two polarizability derivatives of a surface OH.

Author contributions: K.N. and R.A.M. designed research, performed research, analyzed data, and wrote the paper.

Reviewers: S.M., University of California, Irvine; and F.P., University of California San Diego.

The authors declare no competing interest.

[1]To whom correspondence may be addressed. Email: ram@caltech.edu.

This article contains supporting information online at https://www.pnas.org/lookup/suppl/doi:10.1073/pnas.1906243117/-/DCSupplemental.

First published January 29, 2020.

of the water OH stretch mode based on a surface-specific velocity−velocity correlation function (49–52). Quantum effects have been shown to cause a redshift of the OH-stretch band by 150 to 200 cm^{-1} (42, 49, 51–53, 64). Paesani and coworkers used centroid molecular dynamics simulations (66, 67), an approximate quantum approach, to treat the redshift (54, 60, 68, 69).

Gaigeot and coworkers calculated the SFG absolute intensities for real and imaginary parts for ssp SFG susceptibilities employing the density functional theory MD simulation (47, 48) and treated the experimental SFG data of Nihonyanagi et al. (25). We plan to discuss elsewhere the relation of the present work to the experimental results of Nihonyanagi et al. (25) involving broad bandwidth infrared laser and to the theoretical calculations of Gaigeot and coworkers (47, 48).

This paper is organized as follows: The theory is described in *Derivation of SFG Expression Using a Relaxation Method* and then specialized to the case of dangling OH bonds in *Case of a Single SFG Peak, Relation to Wei and Shen*, Eq. **28**. The expression for the SFG susceptibility $\chi^{(2)}(\omega)$ is shown to reduce to the fast and slow limits of Wei and Shen (3) in *Slow and Fast Limits for the Orientational Motion*. A Kubo-like formalism is introduced in *A Kubo-Like Model*, leading to the final results for the absolute integrated susceptibilities (57, 70). The results of the computations are given in *Results*, including a justification in *Justification for Using the Integrated Spectrum*, by adapting the Kubo theory of line broadening, for using the integrated spectrum of a band to circumvent the MD-induced line broadening. The results are discussed in *Discussion*, and concluding remarks are given in *Concluding Remarks*.

Theory

In the present derivation of an expression for the correlation function for SFG using a relaxation method, we neglect for our specific purpose the off-resonant terms, although the method is not restricted to this case. The contribution of the neglected cross-term is about 20% (58). The orientational motion is treated classically, while the vibrational motion of the OH oscillator is treated quantum mechanically in a way that permits introducing infrared and Raman experimental data to calculate absolute SFG intensities. The use of Raman and infrared data was prompted by the work of Wei and Shen (3, 71).

Derivation of SFG Expression Using a Relaxation Method. We consider the resonant SFG polarization in the system with components $P_i^{(2)}(t)$ that result from the visible and infrared laser fields, denoted by E_1 and E_2, respectively, with components E_{1j} and E_{2k}. In terms of a response function $\phi'_{ijk}(t)$ we have

$$P_i^{(2)}(t) = \epsilon_0 \sum_{jk} \int_{-\infty}^{t} \int_{-\infty}^{t} \phi'_{ijk}(t-t_1, t-t_2) \times E_{1j}(t_1) E_{2k}(t_2)\, dt_1\, dt_2, \quad [1]$$

where i, j, k in subscript form refer to the Cartesian directions and ϵ_0 is the electric permittivity of free space. In Eq. **1**, we treat the response to the high-frequency (visible) component E_{1j}, a highly off-resonant response, to be instantaneous and so write

$$\phi'_{ijk}(t-t_1, t-t_2) = \phi_{ijk}(t-t_2)\delta^+(t-t_1), \quad [2]$$

where $\delta^+(\tau)$ is a delta-like function over the semiinfinite τ-domain (0,∞) rather than the usual (−∞, ∞) for a delta function. So $\int_{-\infty}^{t} f(t_1)\delta^+(t-t_1)\,dt_1 = f(t)$. To obtain the ϕ_{ijk} in Eq. **2**, we introduce a relaxation method by setting the infrared-like field $E_{2k}(t)$ equal to a constant E_{2k} prior to $t = 0$ and zero for $t > 0$ and setting Raman-like $E_{1j}(t) = E_{1j}$, a constant for the entire time. Hence, for $t > 0$ we have

$$P_i^{(2)}(t) = \epsilon_0 \sum_{jk} E_{1j} E_{2k} \int_{-\infty}^{0} \phi_{ijk}(t-t_2)\, dt_2, \quad t > 0. \quad [3]$$

Setting $\tau = t - t_2$, Eq. **3** becomes

$$P_i^{(2)}(t) = \epsilon_0 \sum_{jk} E_{1j} E_{2k} \int_{t}^{\infty} \phi_{ijk}(\tau)\, d\tau, \quad t > 0. \quad [4]$$

We next consider the statistical mechanics of this system, a system where as above the "infrared field" is set equal to zero for $t > 0$ and the "visible field" is the same throughout. We have (3, 72)

$$P_i^{(2)}(t) - P_i^{(2)}(\mathrm{eq}) = A^{-1} \sum_{jk} \sum_{n} \ll n|a_{ij}(0) E_{1j} \rho_k(t) \rho_n|n \gg_\Gamma, \quad t > 0, \quad [5]$$

where the sum is over the quantum states $|n>$ of the OH stretching quantized vibrations and A is the surface area. The "n" denotes the totality of quantum numbers for the N molecules. The canonical probability density for these states is denoted in Eq. **5** by ρ_n. The $\ll\gg_\Gamma$ includes an integration over the phase space Γ of the remaining coordinates and momenta, treated classically. The term $a_{ij}(0)E_{1j}$ is the polarizability-induced response to $E_{1j}(t)$, and $\rho_k(t)$ is the time-evolving phase space density in Γ phase space. The value of $\rho_k(t)$ at $t = 0$ is $\rho_k(0)$ and $\rho_k(t)$ evolves in time for $t > 0$ according to the unperturbed Liouville operator L,

$$\rho_k(t) = \mathrm{e}^{-iLt} \rho_k(0), \quad t > 0. \quad [6]$$

Here, the commutator operator L is $[H, \bullet]/\hbar$, where H does not contain the effect of E_{1j}. Both ρ_k (0) and L contain the effect of the constant "visible" field E_{2k} (interacting with the electronic polarizability). We use a mixed classical and quantum mechanical description for the OH stretching vibration and a classical mechanical description for all remaining coordinates (36, 57). We include the time-varying interaction between these two sets of coordinates.

The Hamiltonian H that appears in the L in Eq. **6**, and so the L itself, contains a mixture of classical Poisson brackets and quantum mechanical commutators. In this way, one can include the fact that the interaction of an OH stretch in the $|0>$ state with the other coordinates is different from that of an OH vibrational $|1>$ state. For $t > 0$ the system relaxes according to Eq. **6**, with the initial ρ, $\rho_k(0)$, given by

$$\rho_k(0) = \frac{\exp(-\beta H - \beta \Delta H_k)}{\sum_n < n|\exp(-\beta H - \beta \Delta H_k)|n > \rho_n}. \quad [7]$$

ΔH_k describes the interaction of the dipole moment with the constant infrared field E_{2k},

$$\Delta H_k = -\sum_j \mu_k E_{2k}, \quad [8]$$

where μ_k is the kth component for the ensemble of SFG-active transition dipoles. Upon expanding the $\exp(-\beta \Delta H_k)$ in powers of ΔH_k, one finds, apart from a time-independent term that will not contribute later to the signal at a finite frequency,

$$P_i^{(2)}(t) - P_i^{(2)}(\mathrm{eq}) = \frac{\beta}{A} \sum_{jk} \sum_{n} \ll n|a_{ij}(0)\mathrm{e}^{-iLt}\mu_k(0) \times \mathrm{e}^{-\beta H}|n \gg_\Gamma \rho_n E_{1j} E_{2k} / \sum_n < n|\mathrm{e}^{-\beta H}|n > \rho_n. \quad [9]$$

The susceptibility is given by (73)

$$P_i^{(2)}(t) - P_i^{(2)}(\mathrm{eq}) = \int_0^\infty \chi_{ijk}^{(2)}(\omega) E_{1j} E_{2k} \mathrm{e}^{i\omega t} dt. \quad \textbf{[10]}$$

Although, as in the definition in Eq. **6**, H contains E_{1j}, we see in Eq. **9** that there already is a product of E_{1j} and E_{2k}. The E_{1j} in H can be omitted since it would contribute to a term cubic in the Es. We note too that $\exp(-iL_0 t)\mu_k(0) = \mu_k(t)$, where $\mu_k(t)$ is a quantum mechanical dipole operator acting on the space of the OH stretching eigenstates $|n>$. We define a quantum $< a_{ij}(0)\mu_k(t) >$ by

$$< a_{ij}(0)\mu_k(t) > = \frac{\sum_n \ll n|a_{ij}(0)\mu_k(t)\mathrm{e}^{-\beta H}|n\gg_\Gamma \rho_n}{A\sum_n < n|\mathrm{e}^{-\beta H}|n > \rho_n}, \quad \textbf{[11]}$$

and then obtain

$$P_i^{(2)}(t) - P_i^{(2)}(\mathrm{eq}) = \frac{\beta}{A} \sum_{jk} < a_{ij}(0)\mu_k(t) > E_{1j} E_{2k}. \quad \textbf{[12]}$$

On comparison of Eqs. **4** and **12** we see that they are equivalent if we set

$$\int_t^\infty \phi_{ijk}(\tau) d\tau = \frac{\beta}{\epsilon_0 A} < a_{ij}(0)\mu_k(t) > . \quad \textbf{[13]}$$

Differentiation with respect to t then yields the desired expression for this response function:

$$\phi_{ijk}(t) = -\frac{\beta}{\epsilon_0 A} < a_{ij}(0)\dot{\mu}_k(t) > . \quad \textbf{[14]}$$

The second-order susceptibility $\chi_{ijk}^{(2)}$ is the Fourier–Laplace transform of $\phi_{ijk}(t)$, since

$$\begin{aligned}\chi_{ijk}^{(2)}(\omega) &= -\frac{\beta}{2\pi\epsilon_0 A} \int_0^\infty \mathrm{e}^{-i\omega t} < a_{ij}(0)\dot{\mu}_k(t) > dt. \\ &= \int_0^\infty \mathrm{e}^{-i\omega t} \phi_{ijk}(t) dt. \end{aligned} \quad \textbf{[15]}$$

Integration by parts yields

$$\begin{aligned}\chi_{ijk}^{(2)}(\omega) = &-\frac{\beta}{2\pi\epsilon_0 A} \mathrm{e}^{-i\omega t} < a_{ij}(0)\mu_k(t) > |_0^\infty \\ &-\frac{i\omega\beta}{2\pi\epsilon_0 A} \int_0^\infty \mathrm{e}^{-i\omega t} < a_{ij}(0)\mu_k(t) > dt. \end{aligned} \quad \textbf{[16]}$$

The correlation function for the first term at $t = \infty$ is zero due to the loss of correlation at $t = \infty$. We then have

$$\begin{aligned}\chi_{ijk}^{(2)}(\omega) = &-\frac{\beta}{2\pi\epsilon_0 A} < a_{ij}(0)\mu_k(0) > \\ &-\frac{i\omega\beta}{2\pi\epsilon_0 A} \int_0^\infty \mathrm{e}^{-i\omega t} < a_{ij}(0)\mu_k(t) > dt. \end{aligned} \quad \textbf{[17]}$$

In Eq. **17**, the first term is the initial value of the time response function, while the second term is the Fourier transform of the time response function and serves as the oscillating part in SFG. The first term in Eq. **17** will form part of the background, and so at any finite frequency ω we consider only the second term:

$$\chi_{ijk}^{(2)}(\omega) = -\frac{i\omega\beta}{2\pi\epsilon_0 A} \int_0^\infty \mathrm{e}^{-i\omega t} < a_{ij}(0)\mu_k(t) > dt. \quad \textbf{[18]}$$

The polarizability-induced response to the E_{1j} electric field $a_{ij}(0)$ and to the E_{2k} electric field $\mu_k(t)$ refers to the entire system.

We rewrite Eq. **18** in terms of its contributions from the various molecules:

$$\chi_{ijk}^{(2)}(\omega) = -\frac{i\omega\beta}{2\pi\epsilon_0 A} \int_0^\infty \mathrm{e}^{-i\omega t} \sum_{I,J} < a_{ij}^I(0)\mu_k^J(t) > dt. \quad \textbf{[19]}$$

The sums are over I and J from 1 to N, the number of chromophores in an illuminated surface area A. When the cross-terms $I \neq J$ in Eq. **19** are omitted and it is noted that the average for every I is the same, we can for notational brevity omit the Is and Js and multiply the result by N and let N_s be the surface density of molecules $N_s = N/A$. Eq. **19** becomes

$$\chi_{ijk}^{(2)}(\omega) = -\frac{i\omega\beta N_s}{2\pi\epsilon_0} \int_0^\infty \mathrm{e}^{-i\omega t} < a_{ij}(0)\mu_k(t) > dt, \quad \textbf{[20]}$$

where for notational convenience we have omitted the I, J superscripts and where the $< a_{ij}(0)\mu_k(t) >$s now denote the values for a single surface molecule, instead of a collection of surface molecules. Then for a typical molecule we now write the operators in the form (72)

$$\begin{aligned} H &= H_0|0><0| + H_1|1><1| \\ \mu_k(0) &= \mu_k'(|0><1| + |1><0|) \\ a_{ij}(0) &= a_{ij}'(|0><1| + |1><0|), \end{aligned} \quad \textbf{[21]}$$

where the a_{ij}' and μ_k' are polarizability and dipole moment matrix elements of the molecule and we treat a system where all of the a_{ij}' and μ_k' are the same. The components of quantum correlation function in Eq. **20** can be expressed as

$$< n|a_{ij}(0)\mu_k(t)|n > = < n|a_{ij}\mathrm{e}^{-iHt/\hbar}\mu_k\mathrm{e}^{iHt/\hbar}|n >, \quad \textbf{[22]}$$

where H is given by Eq. **21**. We insert the completeness relations for the chromophore, $\sum_l |l><l|$ and $\sum_m |m><m|$, into the quantum correlation function and so Eq. **22** can be expressed as

$$\begin{aligned} < n|a_{ij}(0)\mu_k(t)|n > = &\sum_{l,m} < n|a_{ij}|l > \\ &\times < l|\mathrm{e}^{-iHt/\hbar}\mu_k|m >< m|\mathrm{e}^{iHt/\hbar}|n >, \end{aligned} \quad \textbf{[23]}$$

where n, l, and m represent the quantum numbers. In SFG experiments, the dangling OH peak involves the transition between 0 and 1 vibrational levels, since the Boltzmann distribution typically has $n = 0$ as the dominant state. l and m in Eq. **22** can be either 0 or 1. According to Eq. **21**, Eq. **23** can be simplified as

$$< n|a_{ij}(0)\mu_k(t)|n > = a_{ij}'\mu_k' e^{-i\omega_q t}, \quad \textbf{[24]}$$

where ω_q denotes the local transitional frequency between ground and first excited vibrational states.

We next rewrite Eq. **20** in terms of direction cosines that transform the expression from molecular space-fixed to molecular body-fixed coordinates, $a_{ij}(0) = \sum_{\lambda\mu} a_{\lambda\mu}(0) D_{i\lambda}(0) D_{j\mu}(0)$ and $\mu_k(t) = \sum_\nu \mu_\nu(t) D_{k\nu}(t)$. We then have

$$\begin{aligned} \chi_{ijk}^{(2)}(\omega) = &-\frac{i\omega\beta N_s}{2\pi\epsilon_0} \int_0^\infty \mathrm{e}^{-i\omega t} \\ &\times \sum_{\lambda\mu\nu} < a_{\lambda\mu}(0)\mu_\nu(t) D_{i\lambda}(0) D_{j\mu}(0) D_{k\nu}(t) > dt, \end{aligned} \quad \textbf{[25]}$$

where the averaging $<>$ in Eq. **25** is over the phase space Γ and the states n, as in the definition given in Eq. **11**. Eq. **25** is applied in various ways, the first of which is to obtain an expression whose slow and fast limits are those given by Wei and Shen (3). Instead

of Eq. **25**, it is customary in the literature to calculate the relative intensities and line shapes, instead of absolute intensities. The equality in Eq. **25** is thereby replaced by a proportionality. So instead the prefactor in the integral in Eq. **25** is omitted (34, 37).

Case of a Single SFG Peak, Relation to Wei and Shen (3). We consider the case of a single SFG peak, in particular, the peak at 3,700 cm^{-1} of a dangling OH group at an air/water interface. We introduce into Eq. **25** the identity operator, $\sum_m |m><m|$, between the operators $a_{\lambda\mu}(0)$ and $\mu_\nu(t)$. The resulting matrix elements of SFG active oscillators can be expanded in powers of the OH oscillator coordinates q for the molecules, retaining the term linear in q for each and noting that only the $m = n+1$ matrix elements contribute to the frequency-dependent signal (the $m = n-1$ would contribute to a signal at a negative frequency). Moreover, at room temperature only the $m = 0$ term contributes for the OH (high frequency) vibration. To minimize the number of symbols in the formalism we now use the notation, $a_{\lambda\mu}(0)$ and $\mu_\nu(t)$, to represent these (0,1) polarizability and dipole quantum mechanical matrix elements. Accordingly,

$$\chi^{(2)}_{ijk}(\omega) = -\frac{i\omega\beta N_s}{2\pi\epsilon_0}\int_0^\infty \mathrm{e}^{-i\omega t} \times \sum_{\lambda\mu\nu} < a_{\lambda\mu}(0)\mu_\nu(t)D_{i\lambda}(0)D_{j\mu}(0)D_{k\nu}(t) > dt. \quad [26]$$

Upon introducing the notation (ω_q, γ_{vib}) of Wei and Shen (3), the operator $\mu_\nu(t)$ can be written as

$$\mu_\nu(t) = \mu_\nu(0)\mathrm{e}^{(i\omega_q - \gamma_{vib})t}, \quad [27]$$

where γ_{vib} is a vibrational damping factor due in part to fluctuations of the OH transition dipole moment. The $\mu_\nu(0)$ and the $a_{\lambda\mu}(0)$ are matrix elements and equal $\sqrt{1/2}a'_{\lambda\mu}$ and $\sqrt{1/2}\mu'_\nu$, respectively, where $a'_{\lambda\mu}$ and μ'_ν denote the derivatives $da_{\lambda\mu}/dq$ and $d\mu_\nu/dq$ (74). Here, q represents the dimensionless OH oscillator coordinate. ω_q denotes local transitional frequency between 0 and 1 local vibrational levels for the water molecule. We take them to be the same for all molecules being considered. We then have

$$\chi^{(2)}_{ijk}(\omega) = -\frac{i\omega\beta N_s}{4\pi\epsilon_0}\int_0^\infty \mathrm{e}^{-i(\omega-\omega_q-i\gamma_{vib})t} \times \sum_{\lambda\mu\nu} a'_{\lambda\mu}\mu'_\nu < D_{i\lambda}(0)D_{j\mu}(0)D_{k\nu}(t) > dt. \quad [28]$$

This expression contains the independently experimentally determined IR and Raman coefficients μ'_ν and $a'_{\lambda\mu}$.

Slow and Fast Limits for the Orientational Motion. The slow and fast motions for the surface dangling OH bonds are the orientational motion of the surface dangling OH bond (S-OH) vs. vibrational relaxation time of the S-OH vibration proposed by Wei and Shen. (3) We next consider the two limiting cases, the slow and fast limits, of Eq. **28** for the orientational motion involved in the $D_{k\nu}(t)$.

The slow limit occurs when the orientational factor $D_{k\nu}(t)$ changes slowly compared with the timescales involved in ω_q and γ_{vib}. One can then replace $D_{k\nu}(t)$ in Eq. **28** by $D_{k\nu}(0)$ and obtain

$$\chi^{(2)}_{ijk}(\omega) = -iN_s\sum_{\lambda\mu\nu} a_{q,\lambda\mu\nu} < D_{i\lambda}(0)D_{j\mu}(0)D_{k\nu}(0) \times \frac{1}{\omega-\omega_q+i\gamma_{vib}} > \quad (\mathrm{Slow}), \quad [29]$$

where we introduced the hyperpolarizability, $a_{q,\lambda\mu\nu}$, defined by

$$a_{q,\lambda\mu\nu} = \frac{\omega\beta}{4\pi\epsilon_0}a'_{\lambda\mu}\mu'_\nu. \quad [30]$$

In the opposite limiting case, the orientational motion of the molecules is fast relative to the timescales involved in ω_q and γ_{vib}. (This case is nonphysical when a high-frequency vibration, such as OH, is involved.) One can average over $D_{k\nu}(t)$ and note that $< D_{k\nu}(t) > = < D_{k\nu}(0) >$. Then Eq. **28** can be written as

$$\chi^{(2)}_{ijk}(\omega) = -iN_s\sum_{\lambda\mu\nu} a_{q,\lambda\mu\nu} < D_{i\lambda}(0)D_{j\mu}(0) >< D_{k\nu}(0) \times \frac{1}{\omega-\omega_q+i\gamma_{vib}} > \quad (\mathrm{Fast}), \quad [31]$$

where $a_{q,\lambda\mu\nu}$ is given by Eq. **30**. Both cases, Eqs. **29** and **31**, were given by Wei and Shen (3).

A Kubo-Like Model. To simulate the change in OH vibrational frequency with environment we use the following Kubo-based oscillator expression (57, 70): For the $\mu_\nu(t)$ appearing in Eq. **25**, we write

$$\mu_\nu(t) = \mu_\nu(0)\exp[i\int_0^t \omega(Q[t'])dt'], \quad [32]$$

where $\omega(Q[t'])$ denotes the dependence of the OH frequency on Q representing the totality of coordinates of the environment of that OH bond. Those Q depend dynamically on the time t, obtained by a molecular dynamics calculation for the ensemble. We may now write Eq. **28** as

$$\chi^{(2)}_{ijk}(\omega) = -iN_s\sum_{\lambda\mu\nu} a_{q,\lambda\mu\nu}\int_0^\infty \mathrm{e}^{-i\omega t} \times < \mathrm{e}^{i\int\omega(Q[t'])dt'}D_{i\lambda}(0)D_{j\mu}(0)D_{k\nu}(t) > dt, \quad [33]$$

where $a_{q,\lambda\mu\nu}$ is shown in Eq. **30** and the limits of the integral over t' are $(0,\ t)$. Estimates of $\omega(Q[t'])$ are given in refs. 57 and 75.

By projecting the OH dynamics from the molecule coordinate onto the laboratory coordinate, Eq. **33** becomes (*SI Appendix*, section A)

$$\chi^{(2)}_{ijk}(\omega) = -iN_s\int_0^\infty \mathrm{e}^{-i\omega t} < \mathrm{e}^{i\int_0^t\omega(Q[t'])dt'} \times \Big\{\Big[a_\parallel(\hat{r}(0)\cdot\hat{\imath})(\hat{r}(0)\cdot\hat{\jmath}) + a_\perp(\hat{\imath}\cdot\hat{\jmath}) - a_\perp(\hat{r}(0)\cdot\hat{\imath})(\hat{r}(0)\cdot\hat{\jmath})\Big][\hat{r}(t)\cdot\hat{k}]\Big\} > dt, \quad [34]$$

where $a_\parallel$ and $a_\perp$ are the hyperpolarizabilities parallel and perpendicular to the OH bond. $\hat{r}(t)$ is the OH bond unit vector. The first and second terms in the square brackets in Eq. **34** represent the Raman scattering process and the infrared absorption process, respectively. The dipole moment derivative is projected to the k direction in the infrared absorption process. In the Raman scattering process, the incident pulse has j polarization. The signal is observed in the i polarization vector. So, the components of the hyperpolarizability should be projected to the j direction and then to the i. For symmetry in the Raman process, the right-hand side of Eq. **34**, $\chi^{(2)}_{ijk}(\omega)$, has exchange symmetry with respect to i and j; i.e., $\chi^{(2)}_{ijk}(\omega) = \chi^{(2)}_{jik}(\omega)$. For a homogeneous water surface, we then have $\chi^{(2)}_{xxz}(\omega) = \chi^{(2)}_{yyz}(\omega)$ and $\chi^{(2)}_{xzx}(\omega) = \chi^{(2)}_{zxx}(\omega) = \chi^{(2)}_{yzy}(\omega) = \chi^{(2)}_{zyy}(\omega)$.

Eq. **34** establishes a connection between the microscopic surface nonlinear susceptibility and the OH bond orientation for each specific water molecule. Eq. **34** and molecular dynamics

simulations are used in the present SFG investigation. Eq. **34** has the surface density of molecules and the absolute intensity of SFG can be derived accordingly. Eq. **34** has the time evolution of the dipole moment where only one temporal orientational projection is involved in each time step. So one can save computer time using this equation, compared with the commonly used equations where the time-dependent correlation functions are derived by calculating the time-dependent polarizabilities (57, 76).

Absolute Intensity of Sum Frequency Generation. The intensity of the SFG in a typical experiment can be derived from Maxwell equations by introducing a thin layer and refractive index $n_i(\omega)$ for medium i at frequency ω (77). It can be written as (71, 78)

$$I(\omega) = \frac{8\pi^3\omega^2 \sec^2\alpha}{c^3 n_1(\omega) n_1(\omega_1) n_1(\omega_2)} |\chi^{(2)}_{\text{eff}}|^2 I(\omega_1) I(\omega_2), \qquad [35]$$

where α represents the output angle for the sum frequency pulse, while $I(\omega_1)$ and $I(\omega_2)$ are the incident pulse intensities.

The second-order susceptibilities in Eq. **15** represent the susceptibilities for the electric field vibrating along the i, j, and k directions for the sum, incident Raman, and incident IR beam, respectively. To relate the $\chi^{(2)}_{ijk}(\omega)$ to the actual experiment, the effective nonlinear susceptibility, $\chi^{(2)}_{\text{eff}}$, for different experimental polarization combinations $\chi^{(2)}_{\text{eff,ssp}}$, $\chi^{(2)}_{\text{eff,sps}}$, and $\chi^{(2)}_{\text{eff,ppp}}$, is written as (71, 78)

$$\chi^{(2)}_{\text{eff,ssp}}(\omega) = L_{yy}(\omega) L_{yy}(\omega_1) L_{zz}(\omega_2) \sin\alpha_2 \chi^{(2)}_{yyz}(\omega) \qquad [36]$$

$$\chi^{(2)}_{\text{eff,sps}}(\omega) = L_{yy}(\omega) L_{zz}(\omega_1) L_{yy}(\omega_2) \sin\alpha_1 \chi^{(2)}_{yzy}(\omega)$$

$$\chi^{(2)}_{\text{eff,ppp}}(\omega) =$$

$$- L_{xx}(\omega) L_{xx}(\omega_1) L_{zz}(\omega_2) \cos\alpha \cos\alpha_1 \sin\alpha_2 \chi^{(2)}_{xxz}(\omega)$$

$$- L_{xx}(\omega) L_{zz}(\omega_1) L_{xx}(\omega_2) \cos\alpha \sin\alpha_1 \cos\alpha_2 \chi^{(2)}_{xzx}(\omega)$$

$$+ L_{zz}(\omega) L_{xx}(\omega_1) L_{xx}(\omega_2) \sin\alpha \cos\alpha_1 \cos\alpha_2 \chi^{(2)}_{zxx}(\omega)$$

$$+ L_{zz}(\omega) L_{zz}(\omega_1) L_{zz}(\omega_2) \sin\alpha \sin\alpha_1 \sin\alpha_2 \chi^{(2)}_{zzz}(\omega),$$

where L denotes the Fresnel factor for the respective electric field. ω, ω_1, and ω_2 are frequencies for output, visible, and infrared pulses, respectively, while α, α_1, and α_2 are the angles that the output, visible, and infrared pulses make with the surface. The other five polarization combinations, sss, spp, pps, psp, and pps have been used to investigate SFG for achiral or chiral elements (79–81).

Results

Experiments Treated. The experimental results that we consider were obtained by Wei and Shen (3), where a 1.5-mJ visible laser pulse at 532 nm and a 100-mJ infrared pulse tunable from 2,900 to 3,850 cm^{-1} (with a linewidth 3 cm^{-1}) were mixed at the water surface with incident angles of 45° and 57°, respectively. Both input pulses had a beam diameter of about 1 mm, a pulse width of about 15 ps, and a repetition rate of 20 Hz. The SFG output was detected in the transmitted direction.

The experimental ssp, ppp, and sps SFG spectra from Wei and Shen (3) for absolute intensity vs. vibrational frequency are illustrated in Fig. 1 *A–C*. The open squares are experimental data and the solid lines are fittings performed by Wei and Shen (3). The SFG peaks can be divided into two groups, where one group has several broad peaks from 3,000 to 3,600 cm^{-1} and the other is a narrow peak from 3,600 to 3,800 cm^{-1}. The narrow peak assigned as a dangling OH bond stretch on the water surface is around 3,700 cm^{-1} (3). The experimental integrated signal for ssp SFG within the dangling OH bond region, from the 3,650- to 3,800-cm^{-1} region, is about 10 times larger than that for ppp and about 40 times larger than that for the sps.

The enlarged and digitized SFG spectra for ssp, ppp, and sps experimental data are shown in Fig. 1 *D–F*, where experimental data and fits by Wei and Shen (3) are illustrated by solid lines and dots, respectively. The baseline for each spectrum is depicted by a dashed line. The fits by Wei and Shen (3) in Fig. 1 *D–F* are the sum of a Lorentzian line shape and this linear background. The Lorentzian implies that the line is homogeneously broadened. For a more direct comparison of the resonant part of the SFG spectra, the baseline removed ssp, ppp, and sps SFG experimental data are shown in Fig. 2, where they are depicted by solid, dashed, and dotted lines, respectively. The peak values for ppp and sps are very small compared with that for ssp and are multiplied by factors 12 and 40 to display comparable areas for the three SFG spectra. The experimental integrated intensities for ssp, sps, and ppp are summarized in Table 1, column 2.

Molecular Dynamics Simulation of Water Surface. The MD simulation of the extended simple point charge (SPC/E) (82) water model was performed using the DL_POLY2 program (83). We used 216 water molecules in a box of 18.7 × 18.7 × 18.7 Å^3, to achieve a density of water molecules at 3.32 × 10^{28}m^{-3} (84). Periodic boundary conditions were employed along the *x*, *y*, and *z* directions. The water molecules are evolved dynamically using an NVT ensemble at the temperature of 300 K for 100 ps. The SHAKE algorithm was used for maintaining the geometry of water molecules (85). The *z* axis was tripled, in that the water is sandwiched between two vacuum phases. A subsequent MD simulation was prepared for a microcanonical ensemble for 10 ns with 0.5-fs time intervals. The snapshots were stored every 1 fs to calculate the time-correlation function in Eq. **34**. As illustrated in figure 1 in ref. 59, two water surfaces were again included. Each water surface is parallel to the *xy* plane and has a random-like shape near the edge of surfaces. It can be seen that some OH

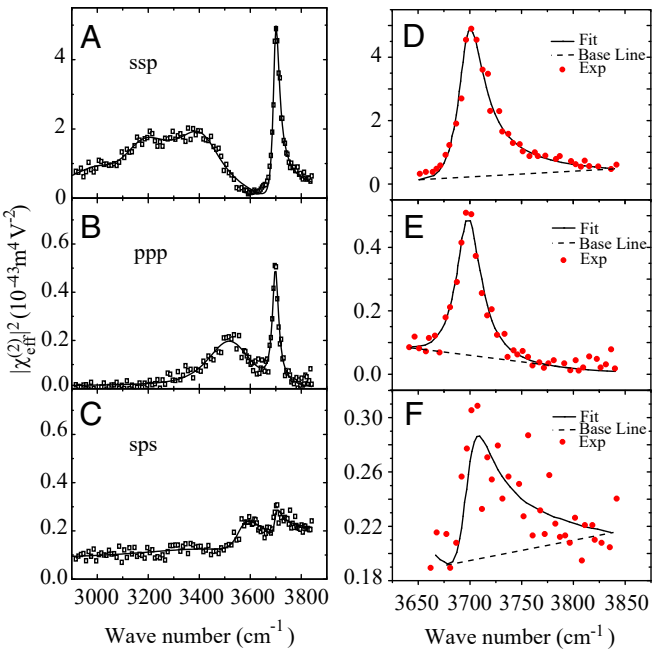

Fig. 1. (*A–C*) ssp, ppp, and sps SFG experimental data from ref. 3. Reprinted with permission from ref. 3. Copyright 2001 by the American Physical Society. (*D–F*) The respective peaks from 3,650 to 3,850 cm^{-1}. The experimental (Exp) data are displayed by the dotted line. The linear baseline for each peak is depicted by a dashed line.

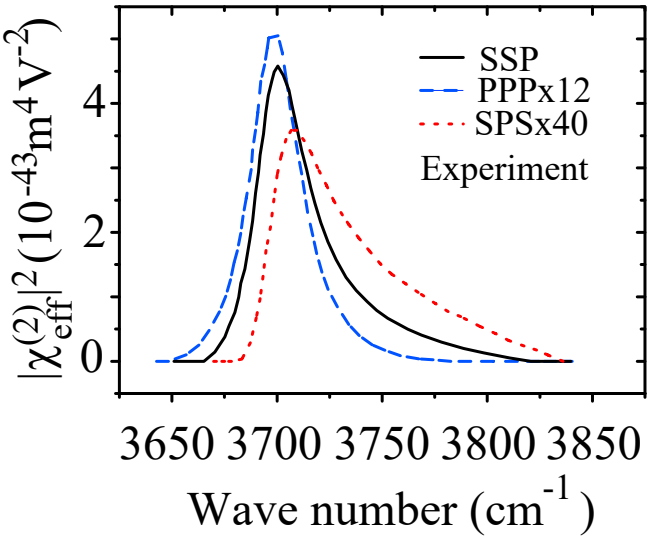

Fig. 2. Baseline removed ssp, ppp, and sps SFG experimental data. To have similar spectral areas in the plot, ssp, ppp, and sps SFG spectra are multiplied by factors 1, 12, and 40, respectively.

bonds are pointing out of the liquid, while others are lying along the *xy* plane or pointing into the liquid.

Sum Frequency Generation Calculation. There are two surfaces with opposite signs of the dipoles. We select the surface of the water molecules where the z coordinates of the oxygens are positive. An empirical correlation between OH bond local mode vibrational frequency in an environment and the local electric field for the SPC/E water model has been given by Auer and Skinner (86), using an equation aimed at selecting the dangling surface OHs,

$$\omega_Q = (3,762 - 5,060E_Q - 86,225E_Q^2)\mathrm{cm}^{-1}, \qquad [37]$$

where E_Q denotes the component of the electric field at the H atom along an OH bond Q. The electric field was calculated in three steps (86): 1) The oxygen atom in a particular water molecule was placed at the center of an *xy* plane. 2) The electric field from the atoms of other water molecules at the position of the H atom was then derived. 3) The electric field was then projected onto the OH bond. The OH local mode frequency is plotted versus the local electric field in Fig. 3 (86), which gives some idea of the scatter along the line given by Eq. **37**. When the nonvanishing element $a_{\|}$ in Eq. **34**, having dipole moment derivative and polarizability derivative terms, is obtained directly from the infrared and Raman spectra experiments for water vapor, the computed absolute integrated intensities are therefore given in Table 1, column 3 (1, 87–90). While it would be more appropriate to introduce instead of the OH data from H_2O vapor the corresponding quantities for a dangling OH bond in a water cluster, a detailed analysis of the latter that provides that information would be needed. A justification for using the integrated spectrum for the comparison with experiment is given in the next section.

The calculated SFG spectra for different polarization combinations, ssp (solid line), ppp (dashed line), and sps (dotted line) of the incident and output pulses are shown in Fig. 4. Some 524,000 trajectories were used in this calculation to reduce noise in the spectrum. The OH stretching vibrational damping factor was chosen as $\gamma_{vib} = 4\ \mathrm{cm}^{-1}$, which corresponds to about 1 ps structure memory time in liquid water (57, 91). As the γ_{vib} is small and has little effect on the integrated spectrum on the SFG, we do not refer this value as an adjustable parameter. To scale similar integrated spectral areas, and so to illustrate their relative areas, the integrated ssp, ppp, and sps SFG intensities were multiplied by factors 1, 74, and 58, respectively. One can see slope baselines for ssp, sps, and ppp in Fig. 4. The calculated spectra whose baselines were removed are shown for the integrated ssp, sps, and ppp SFG spectra in Table 1, column 3.

Justification for Using the Integrated Spectrum. The use of classical trajectories has consistently led to inhomogeneously broadened spectra instead of to the experimentally observed Lorentzian spectrum, as seen in Table 2 (Table 2 also gives references), except in one case where an averaging was made over the fluctuations (41). Rather than using peak intensity to compare with experiment we compare instead the integrated spectra since, as is shown below, assuming the Kubo theory for spectral line shapes, the use of the spectrum integrated over the desired band (here, the 3,700-cm^{-1} band) yields a result that is independent of the extent of inhomogeneous broadening.

We use a functional form for the spectral intensity $I(\omega)$ obtained by Kubo et al. (70), which in the appropriate limits reduces to a Lorentzian for homogeneous broadening and to a Gaussian for inhomogeneous broadening,

$$I(\omega) = \frac{C}{2\pi}\int_{-\infty}^{\infty}\phi(t)e^{-i\omega t}dt, \qquad [38]$$

where $\phi(t)$ is given by

$$\phi(t) = \exp(i\omega_0 t)\exp\left[-t_c\Delta\left(\frac{|t|}{t_c} - 1 + e^{-|t|/t_c}\right)\right]. \qquad [39]$$

Here, ω_0 is the frequency at the peak of the spectrum band, and t_c is the correlation time for the spectral fluctuations

$$t_c = \frac{1}{<\omega_1^2>}\int_0^{\infty} <\omega_1(t_0)\omega_1(t_0+t)>dt, \qquad [40]$$

and Δ is the root-mean-square fluctuation in the frequency:

$$\Delta^2 = <\omega_1^2>. \qquad [41]$$

We have introduced in Eq. **38** a constant C, which is later evaluated by comparing the Lorentzian limit of $I(\omega)$ with the Lorentzian given for the SFG expression by Wei and Shen (3).

The integral over the spectral band is

$$\int_{-\infty}^{\infty} I(\omega)d\omega = C\phi(0) = C, \qquad [42]$$

and so has the same value, regardless of whether the spectrum is Lorentzian, Gaussian, or in between.

Table 1. Experimental vs. theoretical integrated SFG spectra for the dangling OH bond region (from 3,600 cm^{-1} to 3,850 cm^{-1}) in units of 10^{-43} $\mathrm{m}^4\cdot\mathrm{V}^{-2}\cdot\mathrm{cm}^{-1}$

Polarizations	Expt	Calc (gas)	Calc (ice/gas)*	Calc (ice/gas)†
ssp	143	190	366	1,610
sps	3.6	3.0	14	60
ppp	11.9	2.1	30	32

Expt, experimental; Calc, calculated.
*From ice phase $a_{\|}/a_{\perp} = 5.6$, from gas phase $a_{\|} = 5.27 \times 10^{-26}$ $\mathrm{m}^4\cdot\mathrm{V}^{-1}\cdot\mathrm{s}^{-1}$.
†From ice phase $a_{\|}/a_{\perp} = 5.6$, from gas phase $a_{\perp} = 1.68 \times 10^{-26}$ $\mathrm{m}^4\cdot\mathrm{V}^{-1}\cdot\mathrm{s}^{-1}$.

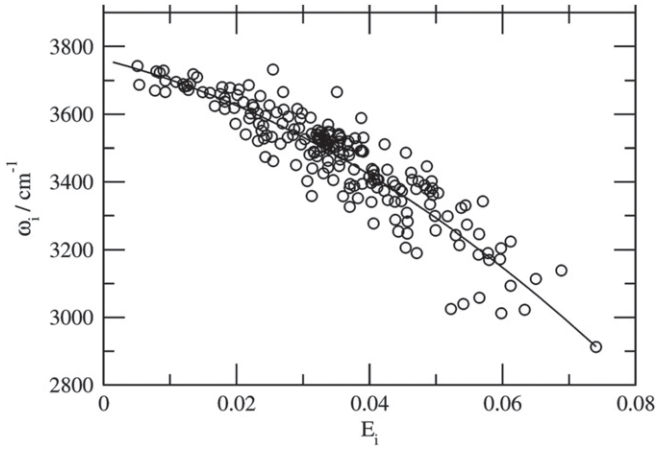

Fig. 3. OH local mode distribution versus electric field proposed by Auer and Skinner (86). Shown is the OH local mode, ω_i, for water clusters vs. electric field E_i in atomic units. The solid curve is the best quadratic fit and the expression is given in Eq. **37**. Reprinted from ref. 86, with the permission of AIP Publishing.

When t_c becomes large, Eqs. **38** and **39** are approximated by a Gaussian

$$I(\omega) = \frac{C}{\sqrt{2\pi\Delta}} \exp\left[-\frac{(\omega-\omega_0)^2}{2\Delta^2}\right]. \quad [43]$$

On the other hand, when t_c becomes small, we have a Lorentzian

$$I(\omega) = \frac{C}{\pi} \frac{e^{\gamma t_c}}{(\omega-\omega_0)^2+\gamma^2}, \quad [44]$$

where

$$\gamma = \Delta^2 t_c. \quad [45]$$

The expression given by Shen and coworkers (71) is

$$I(\omega) = \frac{N_s^2 a_q^2}{(\omega-\omega_0)^2+\gamma^2}, \quad [46]$$

where a_q is the amplitude of the dangling OH vibrational mode. Comparison of Eqs. **44** and **46** yields a value for C.

Discussion

Eq. **36** is used for the final results of the SFG spectra. As the susceptibilities are defined for the unit area, one needs to take into account the surface density, $36/18.7^2$ Å^{-2} in the calculation. Both ssp and sps have one term and the calculated ssp and sps agree, as seen in Table 1, with the experimental data within a factor of 1.3. The ppp has four terms and so is more complex and agrees less well with experiment. Their physical meaning can be explained as follows. In $\chi^{(2)}_{\mathrm{eff,ssp}}(\omega)$, the s that is along the surface has the contribution from x and y in the susceptibility and the p polarized infrared pulse has strong contributions from the OH bond perpendicular to the surface, z direction. The sum and visible beams both have the same polarization, s. Those two factors contribute to ssp being large.

The sps SFG component is small, both experimentally and in the calculations, a result also readily understood: The outgoing SFG and the incoming visible beams now have their electric-field vectors in planes perpendicular to each other, and the IR beam has its electric-field vector in a plane perpendicular to the main direction of the dangling OH bonds. The relatively small value for sps is seen in experiment (3, 18, 28) and is also seen in computations by many authors (36, 37, 41, 61).

In the ppp process, the sum frequency, visible, and infrared pulses are all p polarized, which means that their electric fields all lie in the same plane, a plane perpendicular to the surface. However, the p polarizations of the fields are not parallel or perpendicular to the water surface, but rather make some angle with it. So, because of the (x, y) degeneracy, the susceptibility has a number of terms in the ppp expression in Eq. **36**. There are positive and negative contributions in the terms $\chi^{(2)}_{xxz}(\omega)$ and $\chi^{(2)}_{xzx}(\omega)$ in ppp, so they contribute to its small value in our calculation.

The experimental SFG spectra obtained by different authors (1–3, 5, 8 during the period 1993 to 2008 were collected by Wang and coworkers (29). Those and more recent data for the full width at half maximum (FWHM) and for the peak position of the dangling OH region from both theory and experiment are given for the ssp polarization combination in Table 2. Ref. 3 represents an accurate measurement of the SFG for both line shapes and intensities from different polarizations and served as standard spectra (29, 92). Our calculated results are compared with the experimental SFG spectra in ref. 3 whose peak and width of ssp SFG are shown in the first row in Table 2. The experimental data from different papers can be categorized into two groups with respect to the bandwidth of the infrared laser. In the first group, the FWHMs of the infrared laser are larger than 10 ps (smaller than 3.3 cm^{-1}), where a narrow bandwidth of the dangling OH band can be observed. For the "broad-band" infrared laser experiments, in the second part, whose FWHMs are smaller than or equal to 2 ps (larger than or equal to 17 cm^{-1}), the measured widths of the dangling OH band are relatively larger. One can see that the experimental SSP SFG spectra with narrow- and broad-band incident lasers have different widths and intensities for the dangling OH peak (3, 25, 26). This difference may be due to the very broad instrumental signal in the broad-band SFG of ref. 25.

In the theoretical part in Table 2 one finds that the widths for ssp SFG are all too large except for the single study that corrects for motional narrowing. The data are shown in the last row of Table 2 (41). In comparing experiment and theory we avoid the problem of correcting for motional narrowing by comparing instead the experimental and computed integrated spectra. Wei and Shen (3) fitted the 3,700-cm^{-1} band to a Lorentzian rather than to a Gaussian and so regarded the band as homogeneously broadened. The justification for comparing instead, in our case, the experimental- and computational-based integrated spectrum is given in *Justification for Using the Integrated*

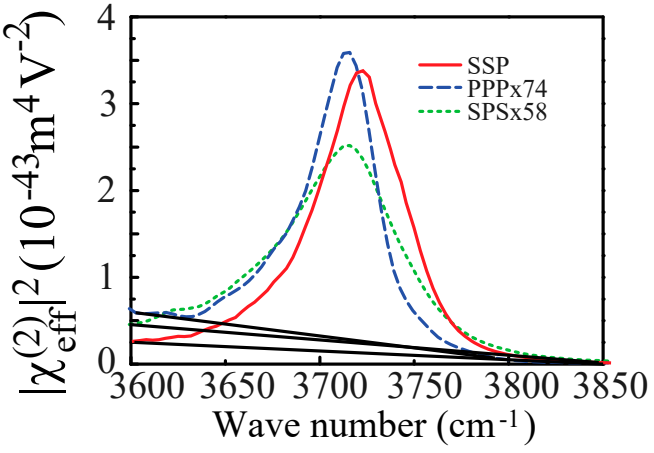

Fig. 4. Calculated SFG spectra for different polarization combinations of the incident and output pulses. To have similar spectral areas (integrated signals) in the plot, ssp, ppp, and sps SFG intensities are multiplied by factors 1, 74, and 58, respectively. The baselines are shown in black.

Table 2. Summary of calculated and experimental peaks and FWHMs for dangling OH bond region of ssp SFG spectra for $|\chi^{(2)}_{ssp}(\omega)|^2$ from different authors

Refs.	Peak (cm^{-1})	FWHM (cm^{-1})
Experiment with infrared laser FWHM >10 ps (<3.3 cm^{-1})		
Wei and Shen (3)	3,700	27
Wang2006 (28)	3,696	35
Shen2008 (5)	3,706	34
Yamaguchi2015 (26)	3,706	29
Shen2016 (7)	3,709	38*
Experiment with infrared laser FWHM ≤2 ps (≥16.7 cm^{-1})		
Richmond2006 (40)	3,708	46
Tahara2015 (25)	3,719	72
Tyrode2018 (30)	3,704	40
Bonn2018 (33)	3,693	48
Theory without motional narrowing		
Hynes2000 (36)	3,653	98
Hynes2002 (64)	3,691†	62
Space2005 (42)	3,701†	108
Richmond2007 (55)	3,692	66
Morita2011 (39)	3,675	60
Skinner2011 (35)	3,704	52*
Gaigeot2013 (46)	3,707	92
Bonn2016 (53)	3,705†	59*
Paesani2016 (54)	3,653	172*
Gaigeot2017 (47)	3,710	100
Our result	3,722	51
Theory with motional narrowing		
Buch/Richmond2007 (41)	3,718	30

The first two sets are the experimental data with the FWHMs of the incident pulses larger than 10 ps and smaller than or equal to 2 ps. The rest are the calculated results.

*In these papers, only the imaginary part was reported. So, the imaginary part is squared. Then, the measured FWHM is multiplied by 1.72 for the width. The 1.72 is the FWHM of $|\chi^{(2)}(\omega)|^2$ over the FWHM of $|\mathrm{Im}(\chi^{(2)}(\omega))|^2$ in our calculation.

†For comparison with the experimental SFG, the calculated results were shifted toward the red by 150 to 200 cm^{-1} in the respective paper.

Spectrum. A method of modifying the computation to convert the inhomogeneously broadened spectrum to a homogeneously broadened one was given by Buch et al. (41). They used a local averaging over a time equal to the correlation time of the fluctuating environment, by averaging over the correlation time of the local electric field. The method introduced by Buch et al. brought the linewidth into close agreement with the experimental value, 30 cm^{-1} vs. 27 cm^{-1}.

In applying the computations to the experimental data, the ratio for the polarizability derivative between the components parallel and perpendicular to the OH bonds for a water molecule is needed. In the gas phase, it is 3.1 and in ice bulk it is 5.6, determined from the ice experimental Raman spectra ratio for the various polarizations relative to the direction of the ice crystal unique axis (93, 94). For comparison with studies of Auer and Skinner (34, 57) whose data were obtained from ice, the SFG spectra were calculated with the ratio of $a_{\|}/a_{\perp} = 5.6$ and values for $a_{\|}$ and $a_{\perp}$ (87–90) taken from gas phase data are shown in in Table 1, columns 4 and 5, respectively. The 3,700-cm^{-1} peak is weak in bulk ice, so the ice has no dangling OH. We chose water vapor for the derivatives principally because bulk ice has no dangling OH bands.

Auer and Skinner (57) tested one aspect of the inhomogeneity by replacing the integration of $\omega(t)$ in the present Eq. **32** by $\omega(0)$. The results for the imaginary part of the SFG susceptibility differed little from those where this approximation was not made. These results by Auer and Skinner (57), seen in their figure 3, confirm that the dangling OH 3,700-cm^{-1} band is, in the MD computations, inhomogeneously broadened, unlike the experimentally observed band, and so has a computed bandwidth (cf. data by many investigations in Table 2) that is much too large.

Wang et al. (59) calculated amplitudes and their ratios of the effective SFG spectra by designating "surface-sensitive" dangling OH bonds on the water surface, where good ratio agreement for ssp:ppp:sps and absolute intensities were reached in the classical MD simulation. However, the intensities varied with different time intervals. In the current work, the SFG intensities are derived using the classical MD simulation with OH local mode vs. electric-field quantum correction. In the current work, identical SFG spectra are reached by performing the calculations with 0.5-, 1-, or 2-fs time intervals in Eq. **34**. So the current calculated results improve the convergence over the earlier work (59).

Space and coworkers (42, 43, 56) developed a time correlation function description of sum frequency generation spectroscopy and the method was applied to theoretically describing the sum frequency generation spectroscopy. The integrated intensity for the dangling OH peak for ssp SFG in figure 1 of Space and coworkers (42) was 1.2×10^{-13} $A^8 \cdot e^2 \cdot K^{-2} \cdot cm^{-1}$, which translates into 1.3×10^{-50} $m^4 \cdot V^{-2} \cdot cm^{-1}$ (details of the calculation are given in *SI Appendix*, section B) which is nine orders of magnitude smaller than the experimental integrated intensity shown in Table 1 (143×10^{-43} $m^4 \cdot V^{-2} \cdot cm^{-1}$). In part, the problem may be due to units.

Wei and Shen et al. (3) used the fast and slow motion effects to describe the very small sps intensity in the experimental data. The equations, Eqs. **29** and **31**, were derived in the current formalism. From our study, where the SFG spectra are derived by using the Fourier transform of the time correlation function of the dipole moment and polarizability derivatives in Eq. **34**, the ratio for ssp:sps can be well reproduced using the general equation, Eq. **34**. The surface dangling OH bond distribution functions studied by Wei and Shen et al. (3) and Wang and coworkers (28) showed that the dangling OH bond was in the fast motion limit. Bonn and coworkers (33) investigated the motional effect using SFG with a broad bandwidth infrared laser and show that the dangling OH bond was in the slow motion limit. We plan to examine this problem elsewhere.

According to the experimental investigation in ref. 31, the effect of the temperature on the dangling OH bond region is small. From our results for the dangling OH stretch region, one expects a small temperature effect for ssp SFG also. The integrated intensity equals an ensemble-averaged product of a molecular dipole moment derivative and polarizability derivative and is largely independent of temperature; other parts of the spectrum will be more sensitive to changes in temperature because of changes in hydrogen bonding arrangements.

Concluding Remarks

The absolute values and the ratios of the integrated SFG intensities for the polarization combination (ssp, sps), whose SFG susceptibilities, each described by a single term, are in reasonable agreement with the experimental results for the integrated intensities within a factor of 1.3 using no adjustable parameters. Using a two-field relaxation treatment, we have derived a sum frequency generation equation for both the line shape and absolute intensity of the second-order susceptibility and also obtained the expressions for the slow and fast limits of the orientational motion first given by Wei and Shen (3).

We have seen (Table 1) that one common choice for the ratio of the perpendicular and parallel polarizabilities, obtained from data on ice, yields a poorer agreement between absolute values for the experimental and calculated intensities than that in the present case found using the gas phase polarizabilities,

perhaps because bulk ice has no 3,700-cm^{-1} band. We have also seen that there is good agreement between the experimental and calculated relative intensities of the two single-term polarization combinations, ssp and sps. The polarization combination ppp has four terms of different and so partially canceling signs and yields, as expected, less good agreement with the calculated value for the integrated intensity.

As summarized in Table 2, the calculations in our work and the investigations by other authors from different papers using various water models, the SPC/E model, and other models can be used to investigate the intensity and line shape of the SFG of dangling OH for the water surface. Extracting the surface structure information can also be used to investigate the SFG (33, 59). According to our present investigations, the motional narrowing effect should be taken into account in further narrowing the FWHM in the calculation. Furthermore, the ssp intensity should be much larger than the sps intensity (36, 37, 41, 61).

Data Availability. The DL_POLY2.0 program was used to calculate the trajectories. All of the data obtained in the present work are given in Figs. 1–4, Tables 1 and 2, and the main text.

ACKNOWLEDGMENTS. We are pleased to acknowledge helpful discussions with Professor Y. R. Shen, Professor S. Mukamel, and Professor Yanting Wang. This work was supported at various times by a number of organizations: the US Army Research Office, the Office of Naval Research, and the James W. Glanville Foundation; and by research grants from Tianjin University of Technology and Education, the Tianjin Municipal Education Commission through Grant JWK1704, and the China Scholarship Council. This work used the Extreme Science and Engineering Discovery Environment, which is supported by National Science Foundation Grant OCI-1053575.

1. Q. Du, R. Superfine, E. Freysz, Y. R. Shen, Vibrational spectroscopy of water at the vapor/water interface. *Phys. Rev. Lett.* **70**, 2313–2316 (1993).
2. Q. Du, E. Freysz, Y. R. Shen, Surface vibrational spectroscopic studies of hydrogen bonding and hydrophobicity. *Science* **264**, 826–828 (1994).
3. X. Wei, Y. R. Shen, Motional effect in surface sum-frequency vibrational spectroscopy. *Phys. Rev. Lett.* **86**, 4799–4802 (2001).
4. Y. R. Shen, *The Principles of Nonlinear Optics* (Wiley, New York, NY, 2002).
5. N. Ji, V. Ostroverkhov, C. S. Tian, Y. R. Shen, Characterization of vibrational resonances of water-vapor interfaces by phase-sensitive sum-frequency spectroscopy. *Phys. Rev. Lett.* **100**, 096102 (2008).
6. Y. R. Shen, Phase-sensitive sum-frequency spectroscopy. *Annu. Rev. Phys. Chem.* **64**, 129–150 (2013).
7. S. Sun *et al.*, Phase reference in phase-sensitive sum-frequency vibrational spectroscopy. *J. Chem. Phys.* **144**, 244711 (2016).
8. S. Baldelli, C. Schnitzer, M. J. Shultz, D. J. Campbell, Sum frequency generation investigation of water at the surface of H2O/H2SO4 binary systems. *J. Phys. Chem. B* **101**, 10435–10441 (1997).
9. D. Simonelli, S. Baldelli, M. J. Shultz, Ammonia water complexes on the surface of aqueous solutions observed with sum frequency generation. *Chem. Phys. Lett.* **298**, 400–404 (1998).
10. D. Liu, G. Ma, L. M. Levering, H. C. Allen, Vibrational spectroscopy of aqueous sodium halide solutions and air liquid interfaces: Observation of increased interfacial depth. *J. Phys. Chem. B* **108**, 2252–2260 (2004).
11. S. Gopalakrishnan, P. Jungwirth, D. J. Tobias, H. C. Allen, Air liquid interfaces of aqueous solutions containing ammonium and sulfate: Spectroscopic and molecular dynamics studies. *J. Phys. Chem. B* **109**, 8861–8872 (2005).
12. L. M. Levering, M. R. Sierra-Hernández, H. C. Allen, Observation of hydronium ions at the air aqueous acid interface: Vibrational spectroscopic studies of aqueous HCl, HBr, and HI. *J. Phys. Chem. C* **111**, 8814–8826 (2007).
13. H. Allen, E. Raymond, G. Richmond, Non-linear vibrational sum frequency spectroscopy of atmospherically relevant molecules at aqueous solution surfaces. *Curr. Opin. Colloid Interface Sci.* **5**, 74–80 (2000).
14. M. Watry, M. Brown, G. Richmond, Probing molecular structure at liquid surfaces with vibrational sum frequency spectroscopy. *Appl. Spectrosc.* **55**, 321A–340A (2001).
15. E. A. Raymond, G. L. Richmond, Probing the molecular structure and bonding of the surface of aqueous salt solutions. *J. Phys. Chem. B* **108**, 5051–5059 (2004).
16. E. A. Raymond, T. L. Tarbuck, M. G. Brown, G. L. Richmond, Hydrogen-bonding interactions at the vapor/water interface investigated by vibrational sum-frequency spectroscopy of "HOD/H2O/D2O" mixtures and molecular dynamics simulations. *J. Phys. Chem. B* **107**, 546–556 (2003).
17. E. A. Raymond, T. L. Tarbuck, G. L. Richmond, Isotopic dilution studies of the vapor/water interface as investigated by vibrational sum-frequency spectroscopy. *J. Phys. Chem. B* **106**, 2817–2820 (2002).
18. T. L. Tarbuck, S. T. Ota, G. L. Richmond, Spectroscopic studies of solvated hydrogen and hydroxide ions at aqueous surfaces. *J. Am. Chem. Soc.* **128**, 14519–14527 (2006).
19. E. Tyrode, C. M. Johnson, A. Kumpulainen, M. W. Rutland, P. M. Claesson, Hydration state of nonionic surfactant monolayers at the liquid/vapor interface: Structure determination by vibrational sum frequency spectroscopy. *J. Am. Chem. Soc.* **127**, 16848–16859 (2005).
20. C. M. Johnson, E. Tyrode, S. Baldelli, M. W. Rutland, C. Leygraf, A vibrational sum frequency spectroscopy study of the liquid- gas interface of acetic acid- water mixtures: 1. Surface speciation. *J. Phys. Chem. B* **109**, 321–328 (2005).
21. E. Tyrode, C. M. Johnson, M. W. Rutland, P. M. Claesson, Structure and hydration of poly (ethylene oxide) surfactants at the air/liquid interface. A vibrational sum frequency spectroscopy study. *J. Phys. Chem. C* **111**, 11642–11652 (2007).
22. P. Viswanath, H. Motschmann, Oriented thiocyanate anions at the air- electrolyte interface and its implications on interfacial water-a vibrational sum frequency spectroscopy study. *J. Phys. Chem. C* **111**, 4484–4486 (2007).
23. P. Viswanath, H. Motschmann, Effect of interfacial presence of oriented thiocyanate on water structure. *J. Phys. Chem. C* **112**, 2099–2103 (2008).
24. H. Du, J. Liu, O. Ozdemir, A. V. Nguyen, J. D. Miller, Molecular features of the air/carbonate solution interface. *J. Colloid Interface Sci.* **318**, 271–277 (2008).
25. S. Nihonyanagi *et al.*, Accurate determination of complex $\chi^{(2)}$ spectrum of the air/water interface. *J. Chem. Phys.* **143**, 124707 (2015).
26. S. Yamaguchi, Development of single-channel heterodyne-detected sum frequency generation spectroscopy and its application to the water/vapor interface. *J. Chem. Phys.* **143**, 034202 (2015).
27. S. Nihonyanagi *et al.*, Unified molecular view of the air/water interface based on experimental and theoretical spectra of an isotopically diluted water surface. *J. Am. Chem. Soc.* **133**, 16875–16880 (2011).
28. W. Gan, D. Wu, Z. Zhang, R. R. Feng, H. F. Wang, Polarization and experimental configuration analyses of sum frequency generation vibrational spectra, structure, and orientational motion of the air/water interface. *J. Chem. Phys.* **124**, 114705 (2006).
29. R. R. Feng, Y. Guo, L. Rong, L. Velarde, H. F. Wang, Consistency in the sum frequency generation intensity and phase vibrational spectra of the air/neat water interface. *J. Phys. Chem. A* **115**, 6015–6027 (2011).
30. S. Sengupta, D. R. Moberg, F. Paesani, E. Tyrode, Neat water-vapor interface: Proton continuum and the nonresonant background. *J. Phys. Chem. Lett.* **9**, 6744–6749 (2018).
31. Y. Nagata *et al.*, The surface roughness, but not the water molecular orientation varies with temperature at the water air interface. *Phys. Chem. Chem. Phys.* **17**, 23559–23564 (2015).
32. W. J. Smit *et al.*, Excess hydrogen bond at the ice-vapor interface around 200 K. *Phys. Rev. Lett.* **119**, 133003 (2017).
33. S. Sun *et al.*, Orientational distribution of free O-H groups of interfacial water is exponential. *Phys. Rev. Lett.* **121**, 246101 (2018).
34. B. M. Auer, J. L. Skinner, Vibrational sum-frequency spectroscopy of the water liquid/vapor interface. *J. Phys. Chem. B* **113**, 4125–4130 (2009).
35. P. A. Pieniazek, C. J. Tainter, J. L. Skinner, Surface of liquid water: Three-body interactions and vibrational sum-frequency spectroscopy. *J. Am. Chem. Soc.* **133**, 10360–10363 (2011).
36. A. Morita, J. T. Hynes, A theoretical analysis of the sum frequency generation spectrum of the water surface. *Chem. Phys.* **258**, 371–390 (2000).
37. A. Morita, Improved computation of sum frequency generation spectrum of the surface of water. *J. Phys. Chem. B* **110**, 3158–3163 (2006).
38. T. Ishiyama, A. Morita, Molecular dynamics study of gas-liquid aqueous sodium halide interfaces. I. Flexible and polarizable molecular modeling and interfacial properties. *J. Phys. Chem. C* **111**, 721–737 (2007).
39. T. Ishiyama, A. Morita, Molecular dynamics simulation of sum frequency generation spectra of aqueous sulfuric acid solution. *J. Phys. Chem. C* **115**, 13704–13716 (2011).
40. D. S. Walker, D. K. Hore, G. L. Richmond, Understanding the population, coordination, and orientation of water species contributing to the nonlinear optical spectroscopy of the vapor-water interface through molecular dynamics simulations. *J. Phys. Chem. B* **110**, 20451–20459 (2006).
41. V. Buch *et al.*, Sum frequency generation surface spectra of ice, water, and acid solution investigated by an exciton model. *J. Chem. Phys.* **127**, 204710 (2007).
42. A. Perry, C. Neipert, C. Ridley, B. Space, P. B. Moore, Identification of a wagging vibrational mode of water molecules at the water/vapor interface. *Phys. Rev. E* **71**, 050601 (2005).
43. A. Perry, C. Neipert, B. Space, P. B. Moore, Theoretical modeling of interface specific vibrational spectroscopy: Methods and applications to aqueous interfaces. *Chem. Rev.* **106**, 1234–1258 (2006).
44. C. J. Tainter, P. A. Pieniazek, Y. S. Lin, J. L. Skinner, Robust three-body water simulation model. *J. Chem. Phys.* **134**, 184501 (2011).
45. Y. Ni, J. L. Skinner, Communication: Vibrational sum-frequency spectrum of the air-water interface, revisited. *J. Chem. Phys.* **145**, 031103 (2016).
46. M. Sulpizi, M. Salanne, M. Sprik, M. P. Gaigeot, Vibrational sum frequency generation spectroscopy of the water liquid–vapor interface from density functional theory-based molecular dynamics simulations. *J. Phys. Chem. Lett.* **4**, 83–87 (2013).
47. S. Pezzotti, D. R. Galimberti, M. P. Gaigeot, 2d H-bond network as the topmost skin to the air–water interface. *J. Phys. Chem. Lett.* **8**, 3133–3141 (2017).
48. S. Pezzotti, M. P. Gaigeot, Spectroscopic BIL-SFG invariance hides the chaotropic effect of protons at the air-water interface. *Atmosphere* **9**, 396 (2018).
49. F. Perakis *et al.*, Vibrational spectroscopy and dynamics of water. *Chem. Rev.* **116**, 7590–7607 (2016).

50. Q. Wan, G. Galli, First-principles framework to compute sum-frequency generation vibrational spectra of semiconductors and insulators. *Phys. Rev. Lett.* **115**, 246404 (2015).
51. T. Ohto, K. Usui, T. Hasegawa, M. Bonn, Y. Nagata, Toward ab initio molecular dynamics modeling for sum-frequency generation spectra; an efficient algorithm based on surface-specific velocity-velocity correlation function. *J. Chem. Phys.* **143**, 124702 (2015).
52. Y. Nagata, T. Ohto, E. H. G. Backus, M. Bonn, Molecular modeling of water interfaces: From molecular spectroscopy to thermodynamics. *J. Phys. Chem. B* **16**, 3785–3796 (2016).
53. J. Schaefer, E. H. G. Backus, Y. Nagata, M. Bonn, Both inter- and intramolecular coupling of O-H groups determine the vibrational response of the water/air interface. *J. Phys. Chem. Lett.* **7**, 4591–4595 (2016).
54. G. R. Medders, F. Paesani, Dissecting the molecular structure of the air/water interface from quantum simulations of the sum-frequency generation spectrum. *J. Am. Chem. Soc.* **138**, 3912–3919 (2016).
55. D. S. Walker, G. L. Richmond, Understanding the effects of hydrogen bonding at the vapor water interface: Vibrational sum frequency spectroscopy of H_2O/HOD/D_2O mixtures studied using molecular dynamics simulations. *J. Phys. Chem. C* **111**, 8321–8330 (2007).
56. A. Perry *et al.*, A theoretical description of the polarization dependence of the sum frequency generation spectroscopy of the water/vapor interface. *J. Chem. Phys.* **123**, 144705 (2005).
57. B. M. Auer, J. L. Skinner, Vibrational sum-frequency spectroscopy of the liquid/vapor interface for dilute HOD in D2O. *J. Chem. Phys.* **129**, 214705 (2008).
58. Y. Nagata, S. Mukamel, Vibrational sum-frequency generation spectroscopy at the water/lipid interface: Molecular dynamics simulation study. *J. Am. Chem. Soc.* **132**, 6434–6442 (2010).
59. Y. Wang, N. O. Hodas, Y. Jung, R. A. Marcus, Microscopic structure and dynamics of air/water interface by computer simulations-comparison with sum-frequency generation experiments. *Phys. Chem. Chem. Phys.* **13**, 5388–5393 (2011).
60. F. Paesani, Getting the right answers for the right reasons: Toward predictive molecular simulations of water with many-body potential energy functions. *Acc. Chem. Res.* **49**, 1844–1851 (2016).
61. D. R. Moberg, S. C. Straight, F. Paesani, Temperature dependence of the air/water interface revealed by polarization sensitive sum-frequency generation spectroscopy. *J. Phys. Chem. B* **122**, 4356–4365 (2018).
62. S. Narayan *et al.*, On water: Unique reactivity of organic compounds in aqueous suspension. *Angew. Chem. Int. Ed.* **44**, 3275–3279 (2005).
63. Y. Jung, R. A. Marcus, On the theory of organic catalysis "on water". *J. Am. Chem. Soc.* **129**, 5492–5502 (2007).
64. A. Morita, J. T. Hynes, A theoretical analysis of the sum frequency generation spectrum of the water surface. II. Time-dependent approach. *J. Phys. Chem. B* **106**, 673–685 (2002).
65. H. L. Friedman, *A Course in Statistical Mechanics* (Prentice-Hall, Englewood Cliffs, NJ, 1985).
66. G. A. Voth, Path-integral centroid methods in quantum statistical mechanics and dynamics. *Adv. Chem. Phys.* **93**, 135–218 (1996).
67. A. Witt, S. D. Ivanov, M. Shiga, H. Forbert, D. Marx, On the applicability of centroid and ring polymer path integral molecular dynamics for vibrational spectroscopy. *J. Chem. Phys.* **130**, 194510 (2009).
68. V. Babin, C. Leforestier, F. Paesani, Development of a first principles water potential with flexible monomers: Dimer potential energy surface, VRT spectrum, and second virial coefficient. *J. Chem. Theory Comput.* **9**, 5395–5403 (2013).
69. V. Babin, G. R. Medders, F. Paesani, Development of a first principles water potential with flexible monomers. II: Trimer potential energy surface, third virial coefficient, and small clusters. *J. Chem. Theory Comput.* **10**, 1599–1607 (2014).
70. R. Kubo, M. Toda, N. Hashitsume, *Statistical Physics II, Nonequilibrium Statistical Mechanics* (Springer Verlag, Berlin/Heidelberg, Germany, ed. 2, 1992).
71. X. Wei, S. C. Hong, X. Zhuang, T. Goto, Y. R. Shen, Nonlinear optical studies of liquid crystal alignment on a rubbed polyvinyl alcohol surface. *Phys. Rev. E* **62**, 5160–5172 (2000).
72. B. M. Auer, J. L. Skinner, Dynamical effects in line shapes for coupled chromophores: Time-averaging approximation. *J. Chem. Phys.* **127**, 104105 (2007).
73. S. Mukamel, *Principles of Nonlinear Optical Spectroscopy* (Oxford University Press, New York, NY, 1995).
74. R. Boyd, *Nonlinear Optics* (Elsevier, Singapore, 1981).
75. K. Nakamoto, M. Margoshes, R. E. Rundle, Stretching frequencies as a function of distances in hydrogen bonds. *J. Am. Chem. Soc.* **77**, 6480–6486 (1955).
76. A. Morita, T. Ishiyama, Recent progress in theoretical analysis of vibrational sum frequency generation spectroscopy. *Phys. Chem. Chem. Phys.* **10**, 5801–5816 (2008).
77. Y. R. Shen, Optical second harmonic generation at interfaces. *Annu. Rev. Phys. Chem.* **40**, 327–350 (1989).
78. X. Zhuang, P. B. Miranda, D. Kim, Y. R. Shen, Mapping molecular orientation and conformation at interfaces by surface nonlinear optics. *Phys. Rev. B* **59**, 12632–12640 (1999).
79. I. Rocha-Mendoza *et al.*, Sum frequency vibrational spectroscopy: The molecular origins of the optical second-order nonlinearity of collagen. *Biophys. J.* **93**, 4433–4444 (2007).
80. L. M. Haupert, G. J. Simpson, Chirality in nonlinear optics. *Annu. Rev. Phys. Chem.* **60**, 345–365 (2009).
81. E. C. Y. Yan, L. Fu, Z. Wang, W. Liu, Biological macromolecules at interfaces probed by chiral vibrational sum frequency generation spectroscopy. *Chem. Rev.* **114**, 8471–8498 (2014).
82. H. J. C. Berendsen, J. R. Grigera, T. P. Straatsma, The missing term in effective pair potentials. *J. Phys. Chem.* **91**, 6269–6271 (1987).
83. W. Smith, T. R. Forester, I. T. Todorov, *The DL_POLY Classic User Manual* (Daresbury Laboratory, Cheshire, UK, 2012).
84. S. A. Corcelli, C. P. Lawrence, J. L. Skinner, Combined electronic structure/molecular dynamics approach for ultrafast infrared spectroscopy of dilute HOD in liquid H_2O and D_2O. *J. Chem. Phys.* **120**, 8107–8117 (2004).
85. J. P. Ryckaert, G. Ciccotti, H. Berendsen, Numerical integration of the Cartesian equations of motion of a system with constraints: Molecular dynamics of n-alkanes. *J. Comput. Phys.* **23**, 327–341 (1977).
86. B. M. Auer, J. L. Skinner, IR and Raman spectra of liquid water: Theory and interpretation. *J. Chem. Phys.* **128**, 224511 (2008).
87. M. Gussoni, Infrared intensities: A new tool in chemistry. *J. Mol. Struct.* **141**, 63–92 (1986).
88. W. Hagen, A. Tielens, J. Greenberg, The infrared spectra of amorphous solid water and ice I_c between 10 and 140 K. *Chem. Phys.* **56**, 367–379 (1981).
89. W. F. Murphy, The rovibrational Raman spectrum of water vapour v_1 and v_3. *Mol. Phys.* **36**, 727–732 (1978).
90. S. A. Clough, Y. Beers, G. P. Klein, L. S. Rothman, Dipole moment of water from Stark measurements of H_2O, HDO, and D_2O. *J. Chem. Phys.* **59**, 2254–2259 (1973).
91. J. A. McGuire, Y. R. Shen, Ultrafast vibrational dynamics at water interfaces. *Science* **313**, 1945–1948 (2006).
92. H. F. Wang, W. Gan, R. Lu, Y. Rao, B. H. Wu, Quantitative spectral and orientational analysis in surface sum frequency generation vibrational spectroscopy (SFG-VS). *Int. Rev. Phys. Chem.* **24**, 191–256 (2005).
93. J. R. Scherer, R. G. Snyder, Raman intensities of single crystal ice I_h. *J. Chem. Phys.* **67**, 4794–4811 (1977).
94. J. E. Bertie, B. F. Francis, J. R. Scherer, On the determination from Raman spectra of the polarizability derivative with respect to the O-H bond stretching coordinate in the ices. *J. Chem. Phys.* **73**, 6352–6353 (1980).